Journal of Physics:
Condensed Matter

PAPER • **OPEN ACCESS**

Spin qubit properties of the boron-vacancy/carbon defect in the two-dimensional hexagonal boron nitride

To cite this article: Sergey Stolbov and Marisol Alcántara Ortigoza 2025 *J. Phys.: Condens. Matter* **37** 385503

OPEN ACCESS
IOP Publishing
Journal of Physics: Condensed Matter
J. Phys.: Condens. Matter **37** (2025) 385503 (8pp)
https://doi.org/10.1088/1361-648X/ae0555

Spin qubit properties of the boron-vacancy/carbon defect in the two-dimensional hexagonal boron nitride

Sergey Stolbov[1,*] **and Marisol Alcántara Ortigoza**[2]

[1] Physics Department, University of Central Florida, Orlando, FL 32816, United States of America
[2] Physics Department, Tuskegee University, Tuskegee Institute, AL 36088, United States of America

E-mail: Sergey.Stolbov@ucf.edu and malcantaraortigoza@tuskegee.edu

Received 12 April 2025, revised 21 August 2025
Accepted for publication 9 September 2025
Published 19 September 2025

Abstract

Spin qubit defects in two-dimensional materials have a number of advantages over those in three-dimensional hosts including simpler technologies for defect creation and control, as well as qubit accessibility. In this work, we select the V_BC_B defect in the hexagonal boron nitride (hBN) as a possible optically controllable spin qubit and explain its triplet ground state and neutrality. In this defect a boron vacancy is combined with a carbon dopant substituting the closest boron atom to the vacancy. Our density-functional-theory calculations confirmed that the system has dynamically stable spin triplet and singlet ground states. As revealed from our linear response GW calculations, the spin-sensitive electronic states are localized around the three undercoordinated N atoms and make local peaks in the density of electronic states within the bandgap. Using the triplet and singlet ground state energies, as well as the energies of the optically excited states, obtained from solution to the Bethe–Salpeter equation, we construct the spin-polarization cycle, which is found to be favorable for the spin qubit initialization. The calculated zero-field splitting parameters ensure that the splitting energy between the spin projections in the triplet ground state is comparable to that of the known spin qubits. We thus propose the V_BC_B defect in hBN as a promising spin qubit.

Supplementary material for this article is available online

Keywords: hexagonal boron nitride, local defect, spin qubit, computational design

* Author to whom any correspondence should be addressed.

1. Introduction

Spin-active local defects in wide-bandgap semiconductors have become a subject of increasingly extensive studies because they are promising building blocks for quantum technology applications. More specifically, in the optically addressable defects, their spin states can be initialized, manipulated, and readout by using optical excitation and emission as well as microwave means. Such defects can serve as spin qubits for quantum computing and sensing. The most known spin-qubit defect is the NV^- negatively charged center in diamond, which combines the nitrogen atom substitution of a carbon next to a carbon vacancy [1, 2]. This defect has a spin triplet ground state and a higher energy local-minimum singlet state. Due to the dipolar spin–spin interaction the triplet spin projections $m_S = 0$ and $m_S = \pm 1$ split (zero-field splitting) (ZFS) within the microwave range energy. If the triplet is optically excited, it undergoes the phonon-assisted intersystem crossing (ISC) transition to an excited state of the singlet configuration. This specific ISC obeys a selection rule in which only triplet states with $m_S = \pm 1$ can transition from the triplet to singlet state. The latter process is followed by the optical emission from the singlet excited to its ground state and the nonradiative transition back to the triplet ground state. Simultaneously, the optical emission from the remaining triplet $m_S = 0$ excited state to its ground state occurs. This spin-polarization cycle thus results in the qubit initialization of the triplet at $m_S = 0$ state [2], which is ready for further optical and microwave manipulation and readout.

The other well-known spin-qubit defects are the negatively charged Si vacancy and the Si–C divacancy in SiC [3, 4]. Although the total spin of the Si vacancy is 3/2, the spin-polarization cycle in these defects is similar to that in the NV^- center. In a recent computational work [5], the authors proposed a new defect with qubit functionality. That is the aluminum-vacancy/sulfur complex (V_BS_N) in the wurtzite AlN. The first-principles evaluation of the electronic structure and optical excitations in V_BS_N indicates that the defect is capable of undergoing the spin-polarization cycle similar to that in the NV^- center.

The above defects are hosted in three-dimensional (3D) semiconductors. Meanwhile, since recently, the search for defect with the spin-qubit functionality has been extended to two-dimensional (2D) systems with a main focus on defects in hexagonal boron nitride (hBN). This is a wide-bandgap (6 eV) layered semiconductor with easily exfoliated monolayers. Hexagonal BN is known, in particular, as a host for single-photon emitters [6]. 2D systems have various advantages over 3D structures. It is easy to create and control the desired defect in 2D hosts and to integrate them into a setup. As for quantum sensing applications, the proximity of a 2D sensor to a sample can significantly increase its sensitivity [7]. The first identified spin defect in hBN with the properties favorable for spin qubit functionality was the negatively charged boron vacancy (V_B^-) [8]. The authors found that V_B^- has a triplet ground state and demonstrated a spin polarization cycle and optical readout. This work has been followed by several experimental and computational studies of this defect [9–11], which revealed that, similar to the Si vacancy in SiC, the polarization cycle does not include and does not require optical emission to the singlet ground state. The defect has a low spin coherence time which results from the interaction of the defect states with the nuclear spin bath of the host atoms. The disadvantage of this spin qubit is its very low quantum yield [9]. Other defects in hBN have been also under consideration. The authors of computational work proposed the carbon tetramer defect in hBN as possible spin qubit [12]. According to their computational results, the tetramer defect has both triplet and singlet states and is capable to undergo a spin polarization cycle. Another recent computational and experimental study [13] reveals that the B asymmetric divacancy also has the triplet and singlet states. However, in this system, the triplet and singlet states are almost degenerate which makes the ISC from the singlet to triplet state forbidden.

In this work we put to the test a V_BC_B defect in hBN. The V_BC_B defect has a vacancy formed by removing a B atom and substituting one of the next nearest B atoms to the vacancy by carbon (C). In section 3.1, a detailed description of the defect will be provided. This defect has been reported to have a triplet and singlet states (database of [14]). However, the authors did not search for the lowest energy singlet state but constrained the system to remain at a desired spin state. In this work, we will show that the total energy of a singlet calculated in such manner may be much larger than that of other singlet configurations. Furthermore, neither the rationale for the V_BC_B triplet ground state, nor its electronic structure, nor the spin-qubit functionality or lack of it has been addressed so far. By applying the existing knowledge, we focus on explaining why the complex combining a boron vacancy and another boron atom substituted by carbon (V_BC_B) has a *neutral* triplet ground state and demonstrates that its properties are suitable for the spin qubit functionality. We perform density-functional-theory (DFT)-based calculations to find the triplet and singlet states and test their dynamical stability. Next, we apply the linear response GW [15] and Bethe–Salpeter equation (BSE) [16] methods to evaluate the defect's electronic structure and optical excitations followed by the construction of the spin-polarization cycle and the calculation of the ZFS.

2. Computational details

To perform the first-principles calculations we used the Vienna *ab-initio* simulation package VASP 6.4 [17] with the projector-augmented-wave potentials [18]. The 400 eV cutoff energy for the plane-wave expansion was used for all calculations. The total energy of the systems and phonon spectra (at the Γ-point) were calculated within DFT with the Perdew–Burke–Ernzerhof approximation for the exchange-correlation functional [19]. Periodicity of the defected system was achieved by using the $5 \times 5 \times 1$ 50-atom supercell. The

Brillouin zone was sampled with the $3 \times 3 \times 1$ k-point mesh. The electronic structure, in terms of the independent quasiparticle (IQP) states, was calculated using the GW method [15] within the GW_0 approximation (3 iterations for Green's function). The obtained GW wavefunctions and kernels are used to calculate the frequency-dependent dielectric functions and oscillator strengths of the optical excitations within the BSE method [16]. Each BSE eigenstate is a result of the summation of multiple transitions from occupied to unoccupied single-particle states. BSE takes into account the electron-hole interaction (excitonic effects).

3. Results and discussion

The first requirement for a spin qubit is that the corresponding defect must have a spin-polarized ground state ($S = 1$ or higher). It is known that, in solids, weak chemical bonds or, better, broken bonds between an atom and its neighbors are favorable for formation of non-zero spin state of the atom. The easiest way to break the bonds and make the neighboring atoms undercoordinated is the creation of a vacancy in crystal. For example, the creation of a B-vacancy in hBN makes three N atoms undercoordinated. And as a result, this defect becomes spin-polarized [8]. However, removal of the B atom reduces the number of valence electrons in the system by one (note that we consider only valence p-electrons and neglect the effects of semi-core 2 s-electrons of B). That would make the number of valence electrons odd leading to a total spin equal to 3/2. If the defect became negatively charged (that is, one extra electron is added to the system) the number of electrons would be even resulting in a 2/2 total spin (triplet). This is the mechanism of formation of a triplet state in the V_B^- defect in hBN. However, once it is understood why boron vacancies occur in a negatively charged state, one can devise another way to bring back the missing valence p-electron, while *keeping the defect electrically neutral*, which is to substitute another host atom with a dopant having a suitable number of the p-valence electrons [5]. Namely, in the case of the V_BC_B defect, the substitution of another B atom with a carbon atom—which has two valence p-electrons—leaves three N atoms undercoordinated and keeps the number of valence p-electrons even while leaving the defect electrically neutral. In this way we explain why the V_BC_B defect has a triplet ground state and is expected to be neutral. The above reasoning to find defects with triplet ground states has a caveat in regard to suitable substitutional dopants. Namely, if the radius of the dopant is significantly larger than that of the host atoms, it is likely that the ground state will be a singlet because the dopant will tend to compress the bonds among the host atoms and prevent the undercoordinated ones to become spin polarized.

3.1. Spin states and stability of the V_BC_B defect

The next steps are to perform the first-principles calculations to a) reveal the equilibrium geometric structure of the defect, b) check if the spin triplet state is the ground state, c) find whether the defect has also a singlet state, and d) evaluate stability of the defect. All these steps involve only electronic ground state processes; therefore, we perform the corresponding calculations within DFT.

Table 1. Formation energy and binding energy of C calculated for the considered defects.

Defect	E_{form} N-rich (eV)	E_{form} N-poor (eV)	E_B (C) (eV)
V_BC_B	+6.577	+11.793	−16.337
V_NC_B	+9.223	+9.223	−12.247

One experimental method for the creation of carbon-doping/vacancy defects in hBN is the carbon ion implantation [20]. In this process, the impact of a ∼10 keV-energy C ion is assumed to cause a B-vacancy accompanied by the substitution of another B atom with the incoming C ion. In light of the above process, we create a supercell with the V_BC_B defect configuration shown in figure 1 and calculate the relaxed defect structure. Indeed, we confirmed that this defect has a triplet ground state. Considering that the C-dopant may take some other positions, we also consider another configuration with carbon substituting the B atom marked in the figure by white cross. We find, however, that the total energy of this configuration is 0.727 eV higher than that of the first configuration, which may be indicative of the role of carbon in a vacancy healing effect. Another option may be that the carbon atom substitutes, not B, but N, creating the V_BC_N defect instead. However, it has been shown earlier that this defect is dynamically unstable and undergoes a transition to the stable V_NC_B defect [21]. In table 1, we thus compare the energetic characteristics of both neutral V_BC_B and V_NC_B defects. We provide the standard formation energy of the defects obtained as:

$$E_{form}(V_BC_B) = E_{tot}(V_BC_B) + 2\mu(B) - E_{tot}(BN) - \mu(C) \quad (1)$$

$$E_{form}(V_NC_B) = E_{tot}(V_NC_B) + \mu(B) + \mu(N) - E_{tot}(BN) - \mu(C) \quad (2)$$

Here, E_{tot}(BN), $E_{tot}(V_BC_B)$ and $E_{form}(V_NC_B)$ are the total energy of the pristine and V_BC_B-and V_NC_B defected hBN structures, respectively; and μ (X) is the chemical potential of X (for X=B, N, and C). Note that in table 1 that for V_NC_B, its formation energies of under N-poor and N-rich conditions are identical. This is expected because the only terms that vary in equation (2), between the N-poor and N-rich conditions, are the chemical potentials μ(B) and μ(N). Nevertheless, their sum μ(B) + μ(N) remains constant and is equal to the chemical potential of the pristine hBN, μ(BN), under both conditions.

The formation energy is a thermodynamic quantity giving the energy of configurations achieved in infinite time. However, experimental defect creation involves not only thermodynamic process but also, and more importantly, a kinetic process. Namely, the lifetime of a thermodynamically unstable defect is a kinetic quantity that depends on the height of the activation energy barrier(s) to reach the most stable configuration, which is determined by the strength of the chemical bonds between the dopant and its neighbors. Therefore, in addition to

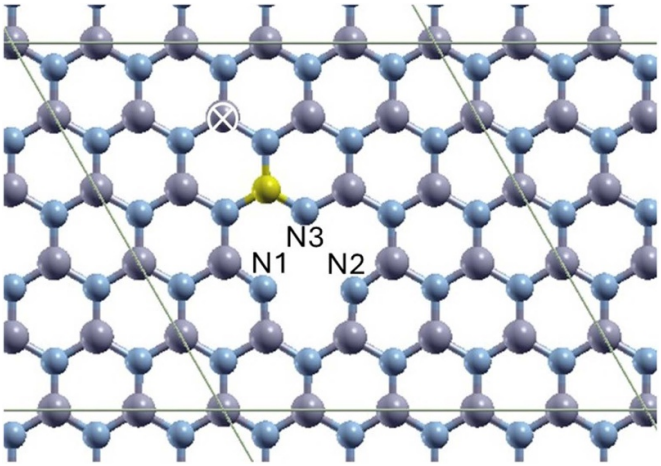

Figure 1. The proposed configuration of the V_BC_B defect. The grey, blue, and yellow balls represent the B, N, and C atoms respectively. N1, N2, and N3 mark three undercoordinated N atoms. The white cross marks the other considered position of the C atom. The bright green lines show the supercell boundaries.

the formation energy, we provide in table 1 the dopant binding energy (E_B) of the defect. For V_BC_B it is

$$E_B(C) = E_{tot}(V_BC_B) - E_{tot}(2V_B) - E_{at}(C) \quad (3)$$

and for V_NC_B

$$E_B(C) = E_{tot}(V_NC_B) - E_{tot}(V_BV_N) - E_{at}(C). \quad (4)$$

Here, $E_{tot}(2V_B)$ is the total energy of defected structure with two B-vacancies and $E_{tot}(V_BV_N)$ is the total energy of defected structure with one B-vacancy and one N-vacancy. The absolute value of the C binding energy in V_BC_B is much higher than that in V_NC_B, indicating, as expected, that breaking C–N bonds requires more energy than breaking C–B bonds does, and hence suggesting that the lifetime of V_BC_B has to be longer than that of V_NC_B. We thus conclude that the V_BC_B defect is energetically more favorable than V_NC_B, and its preferred structure is the one shown in figure 1. Note that, due to the presence of the C dopant, the defect has an asymmetric structure in which, in contrast to the V_B defect [8], the N1, N2, and N3 atoms are nonequivalent. To test the dynamic stability of V_BC_B, we calculate its phonon spectrum. We find that there is no vibrational mode with imaginary frequency, which indicates that the defect is dynamically stable.

To find a singlet state of V_BC_B we start with the relaxed triplet structure and re-relax it without spin polarization. Then, we used the obtained structure as the input to rerun the structural relaxation with the spin polarization on. From our experience this is an efficient way to obtain the lowest energy singlet. As a result, we obtained the system in the singlet states with total energy 0.043 eV higher than that of the triplet state. The phonon spectrum of the singlet confirms that it is also dynamically stable. To test the accuracy of the results we calculated both triplet and singlet DFT total energy for the smaller 4×4 supercell. We found that for the 4×4 case the difference between total energy of the triplet and singlet is 0.0435 06 eV,

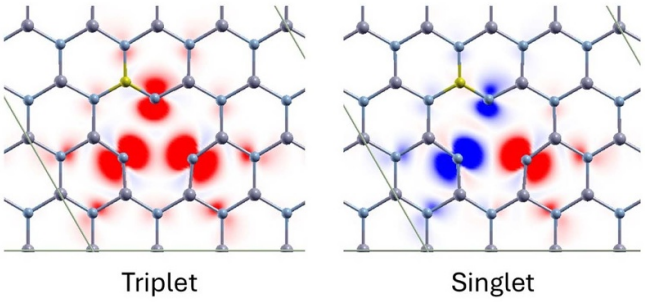

Figure 2. The in-plane cut of the spin density calculated for the triplet and singlet states of the V_BC_B defect. The red and blue areas correspond to the spin-up and spin-down densities, respectively.

while for the 5×5 supercell it is 0.0431 5 eV. Moreover, the DFT total density of state (DOS) of the 6×6 supercell is almost identical to that of the 5×5 supercell. We thus conclude that the 0.043 eV obtained for the 5×5 supercell is a reliable number for the energy difference. Figure 2 illustrates the spin density distribution in the V_BC_B defect. As expected, the spin density is mostly localized around the undercoordinated N atoms. Interestingly, although the total spin of the singlet state is zero, the three undercoordinated N atoms are spin-polarized with the spin-up and spin-down contributions compensating each other. It is worth noticing that we also calculated a singlet state with the 'closed-shell' configuration with zero-spin on each atom and found its energy to be 0.38 eV higher than that with spin-polarized N atoms. This result was expected. The balance between the binding energy and exchange energy for undercoordinated N atoms is in favor of spin polarization because of the presence of dangling bonds.

3.2. Electronic structure and optical excitations in the V_BC_B defect

We found that the V_BC_B defect has a triplet ground state, as well as a singlet state with higher total energy. This is a necessary but not sufficient condition for the spin qubit functionality. The spin-polarization cycle is a process involving the excited states of the system, which we evaluate next. Since DFT fails to account for the excited states, we move at this point to the advanced GW and BSE methods which are sufficient to describe the properties in question.

To test the accuracy of our GW settings and have a system of reference for the defect, we calculate the electronic structure of the pristine hBN by applying the GW method. Next, we use the GW wavefunction as an input for the BSE method to calculate the optical excitation spectrum for this material. Figure 3 shows the imaginary part of the frequency-dependent dielectric function which reflects the energetics and structure of the optical absorption spectrum. We find our results to be in excellent agreement with the experimental absorption spectra: namely, the main peak located is at 6 eV [22, 23] and the second one at 7 eV [23]. Another test we performed was the one on accuracy with respect to the supercell size. In section 3.1. we report a negligible effect of the supercell size ($4 \times 4 \times 1$, $5 \times 5 \times 1$, and $6 \times 6 \times 1$) on the difference in

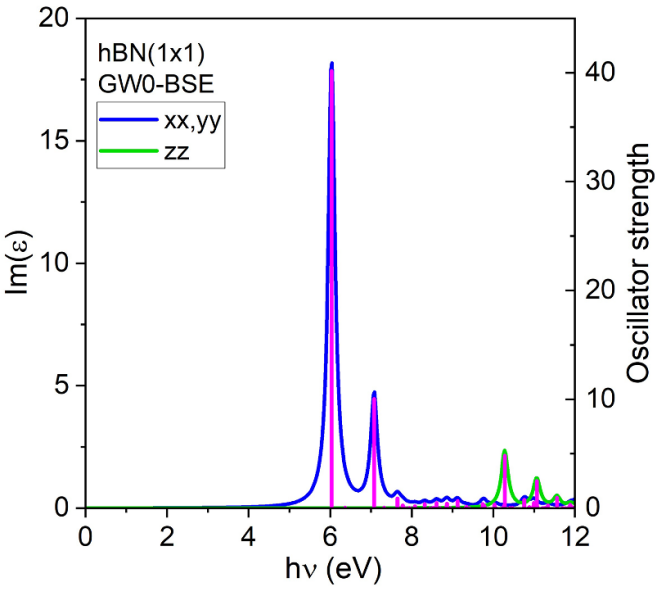

Figure 3. The imaginary part of the dielectric function (blue and green lines) and oscillator strength calculated for the pristine hBN monolayer by GW-BSE method.

total energies of triplet and singlet. That was a ground state evaluation. We also tested the supercell size effect on optical excitations of the defect. The results provided as supplementary data show that the error in energy position of a dielectric function peak of interest due to finite supercell size does not exceed 0.15 eV.

Next, the GW calculations were performed for the triplet and singlet states of the V_BC_B defect. As seen from figure 4, in contrast to the pristine hBN (figure 3), extra peaks related to the V_BC_B defect appear in the DOS. The occupied peaks are located just above the valence band (VB) within ∼1 eV below the Fermi level while the unoccupied ones are positioned within the bandgap, approximately 4 eV above the Fermi energy. As seen from figure 2, the spin polarized states for both triplet and singlet are formed around the undercoordinated N atoms: N1, N2, and N3. From the shape of the spin-density lobes, we conclude that they are formed upon an in-plane hybridization of the *p*-electron states of these atoms. To reveal their contribution to the total DOS of the system we analyze the local densities of the *p*-states of the N1, N2, and N3 atoms. As shown in figure 5, the occupied *p*-states of the N1 and N2 atoms form a wide low-density band reflecting their hybridization with the VB states, as well as narrow peaks corresponding to relatively isolated (not hybridizing) states just above VB, which are mostly responsible for the spin polarization in V_BC_B. The *p*-states of N3 exhibit an enhanced peak between 1 and 3 eV below the Fermi level, which corresponds to a strong hybridization with the neighboring C atom causing the reduced spin polarization at the N3 atom. In the singlet case, the *p*-states of the undercoordinated N atoms form extra sharp occupied DOS peaks at 2 eV below the Fermi level in addition to the states between −1 and 0 eV. We conclude that, even though the peaks at −2 eV overlap with host's VB, their sharpness tells us that there is no significant hybridization. Consequently, the peaks at −2 eV contribute to the local spin polarization of the singlet. The narrow unoccupied DOS peaks are also associated with the *p*-states of the N1, N2, and N3 atoms for both triplet and singlet. Such an electronic structure seems to be favorable for sharp-peak optical excitation and emission. Thus, the next step is focused on the optical properties of the V_BC_B defect.

We apply the BSE method to calculate the frequency-dependent dielectric function and oscillator strength of optical dipole excitations for the triplet state of V_BC_B. The results are shown in the left panel of figure 6. We find that a sharp excitation peak is formed in the triplet at an energy of about 3.2 eV. It is worth mentioning that the triplet first excitation energy obtained in Ref. 14 using the HSE06 hybrid functional was reported to be ∼ 3.55 eV. Our HSE06 optical spectrum (not provided here) is in agreement as it gives 3.7 eV. Noticeably, the ratio of the *xx*–*yy*-polarization oscillator strengths is about 40% for all three calculations mentioned above. This transition has an oscillator strength comparable or higher than that of other defects in hBN that we studied earlier [21]. This excitation is the first step of the spin-polarization cycle. The next step is expected to be a phonon-assisted ISC to a singlet state. It cannot occur directly from the excited triplet state to the ground singlet state because of the large difference in energy (about 3 eV). However, it can proceed through some singlet excited state, as happens in the NV^- center. To obtain the singlet excited states we use the BSE method to calculate its optical excitation spectrum. The results are shown in the right panel of figure 6. We find the singlet to have several sharp defect-related excitation peaks. The peak at 2.46 eV corresponds to the singlet excited state that may contribute to the spin-polarization cycle.

3.3. Spin-polarization cycle proposed for the V_BC_B defect

We find out from our calculations that the V_BC_B defect has stable triplet and singlet states and that the total energy of the singlet ground state is 0.044 eV higher than that of the triplet ground state. Our BSE calculations indicate that the singlet has excited states with energy lower than those of the triplet. These conditions are favorable for the spin-qubit optical initialization via the cycle described in the Introduction. We thus construct the spin-polarization cycle for V_BC_B (see figure 7). The first step in the loop is the optical excitation from the triplet ground state to the triplet excited state. We find two excitations relevant to the loop with energies around 3.2 eV. This excitation will require a UV laser. Next, we can expect the system to undergo the phonon-induced ISC from the triplet excited to the singlet excited state with $m_S = \pm 1$ (Via a selection rule) followed by emission to the singlet ground state and then another ISC to the triplet ground state. As seen from figure 7, the relative energies of the states involved in the process make the spin-polarization cycle viable.

This is an important finding predicting that the V_BC_B defect may have a qubit functionality. The critical quantities determining the spin-polarization cycle are energies of the ground and optically excited states of the triplet and singlet states of the defect. In contrast to ground state, the

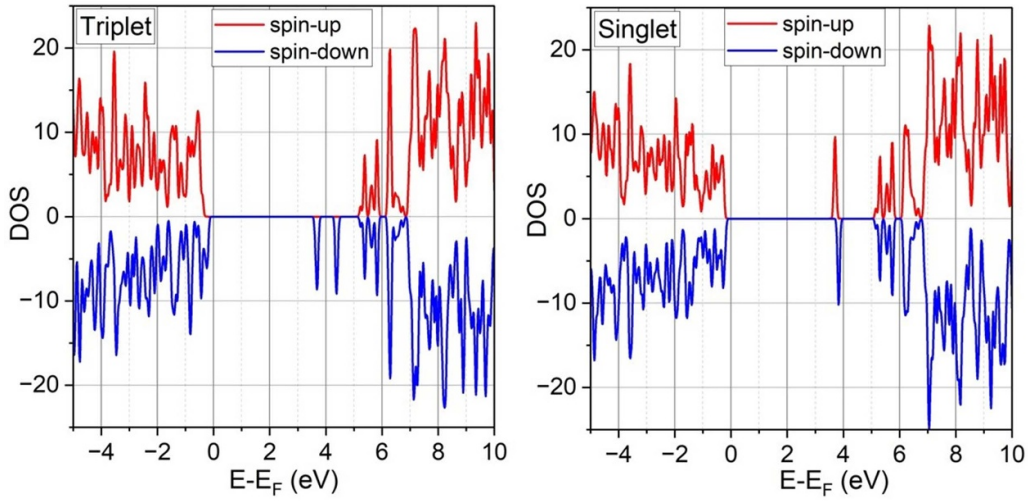

Figure 4. Density of the IQP states calculated for the triplet and singlet state of the V_BC_B defect.

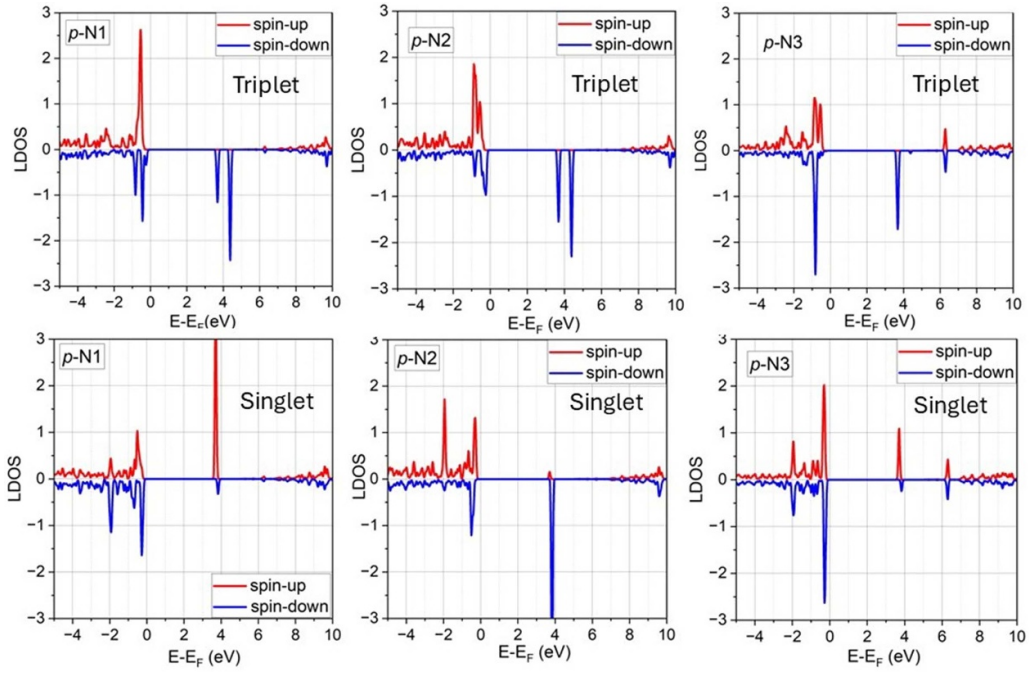

Figure 5. Local densities of the p-states of the undercoordinated N atoms calculated for the triplet and singlet in the V_BC_B defect.

excited state calculations require very complicated computational techniques, and it is important to be confident in their reliability. Therefore, we performed additional calculations of the energies of the ground and excited states of V_BC_B using an alternative to GW-BSE, time-dependent DFT (TDDFT) method based on the hybrid functional. Our comparison to the GW-BSE results reveals that the TDDFT excited states energies differ from those of GW-BSE by 0.4–0.5 eV. However, the TDDFT energy values are such that the spin-polarization cycle is feasible, as it is for the GW-BSE prediction. The results of the TDDFT calculations are provided as supplementary data.

The proposed cycle in the V_BC_B defect may be more efficient for technological applications than that in the V_B^- defect. Namely, the high rate of the ISC from the triplet excited to the singlet excited states of V_B^- has been found to be responsible for short triplet excited-state lifetime and its very low quantum yield [9]. This has been supported by calculations presented in [11]. The authors found that the triplet to singlet excited-state transition has a rate several orders of magnitude larger rate than that calculated for the triplet's optical decay for the $m_s = 0$ spin projection. Importantly, they traced the high rate of the ISC from the triplet excited to the singlet excited state to their near degeneracy and their similar

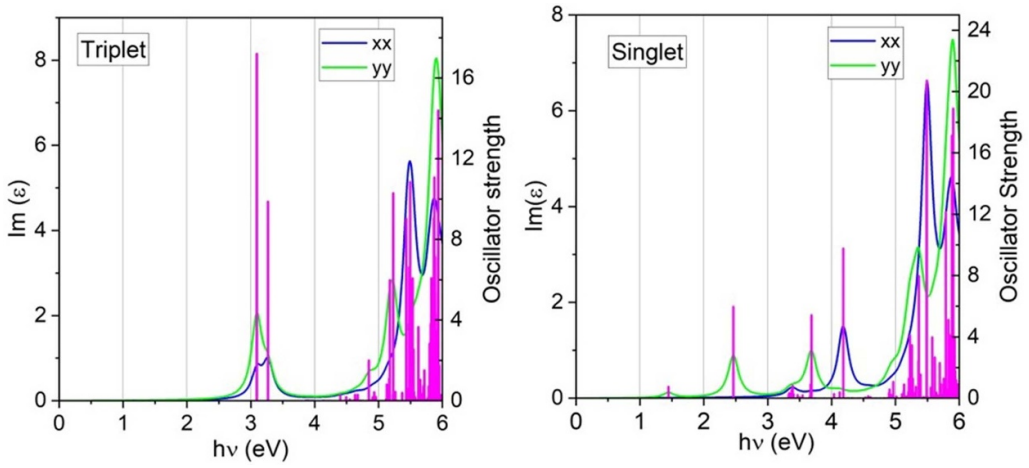

Figure 6. The frequency-dependent dielectric function (blue and green lines) and the oscillator strength (pink bars) calculated for the triplet and singlet spin states in the V_BC_B defect. The zz-polarization of Im(□) is not shown because its magnitude is negligible.

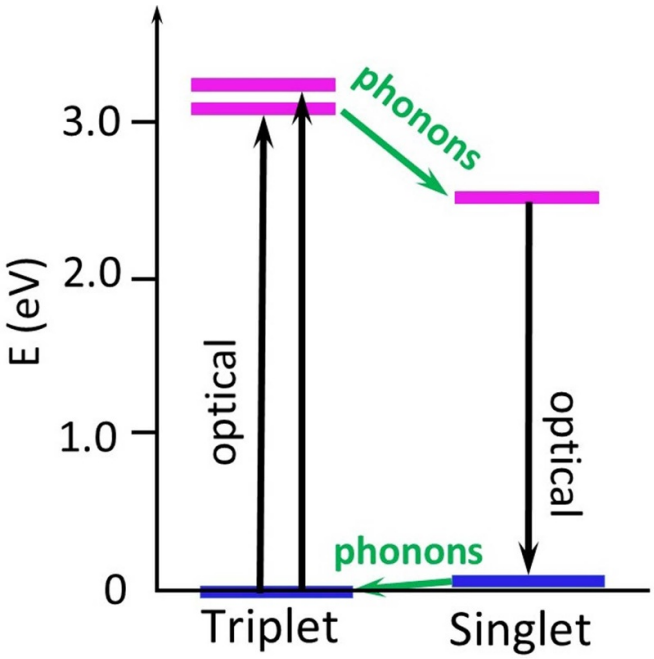

Figure 7. The proposed energy diagram for the spin-polarization cycle in the V_BC_B defect. The blue and pink bars indicate the ground and excited states, respectively.

structure. According to our results, the triplet and singlet excited states in the V_BC_B defect are energetically separated by about 0.5 eV, which prevents the high rate of ISC. Therefore, we expect the spin qubit initialization to be more efficient in V_BC_B than in V_B^-. Another important characteristic of spin qubits is the ZFS, which is the splitting between the triplet spin projections caused by the dipolar spin–spin interaction. We calculated the ZFS parameter D for the triplet ground state and found it to be equal to 2.706 GHz. This value is comparable to the ZFS parameters obtained for the V_B^- $D = 3.48$ GHz [10], and NV^- defects $D = 2.88$ GHz [1], indicating that the spin polarization manipulation is feasible as it is for other studied defects. We thus conclude that the proposed V_BC_B defect in hBN has properties favorable for the qubit functionalities including its initialization, manipulation, and readout.

4. Conclusions

By applying the existing knowledge and an educated guess, we proposed the V_BC_B defect in hBN as a possible spin qubit. Our DFT calculations confirmed that the defect has stable triplet and singlet ground states, and that the latter has a total energy 0.044 eV higher than the former, which is favorable for the spin-qubit functionality. We found from our GW calculations that the spin-active electronic states associated with the defect are localized around the undercoordinated N atoms and create sharp peaks in the density of electronic states within the bandgap. The frequency-dependent dielectric function and oscillator strength have been calculated for the triplet and singlet within the BSE method. We found from these calculations that the optical excitations in both the triplet and the singlet have energies and rates favorable for the spin-polarization cycle. Using the data obtained for the ground and excited state energy, we constructed a spin-polarization-cycle diagram. This diagram, along with the result of the ZFS calculations, indicates that the V_BC_B defect has promising spin qubit functionalities.

Data availability statement

All data that support the findings of this study are included within the article (and any supplementary files).

Acknowledgments

This work was supported by the U.S. Department of Energy, Office of Science, Basic Energy Sciences, under Award # DE-SC0024487.

ORCID iDs

Sergey Stolbov 0000-0002-5687-0457
Marisol Alcántara Ortigoza 0000-0003-3579-4894

References

[1] Doherty M W, Manson N B, Delaney P, Jelezko F, Wrachtrup J and Hollenberg L C L 2013 The nitrogen-vacancy colour centre in diamond *Phys. Rep.* **528** 1–45
[2] Gali A 2019 *Ab initio* theory of the nitrogen-vacancy center in diamond *Nanophotonics* **8** 1907–43
[3] Koehl W, Buckley B, Heremans F, Calusine G and Awschalom D D 2011 Room temperature coherent control of defect spin qubits in silicon carbide *Nature* **479** 84–87
[4] Widmann M *et al* 2015 Coherent control of single spins in silicon carbide at room temperature *Nat. Mater.* **14** 164–8
[5] Stolbov S and Alcántara Ortigoza M 2024 Aluminum vacancy/sulfur complex in wurtzite AlN as an optically controllable spin qubit *Phys. Rev. B* **109** L241108
[6] Tran T T, Bray K, Ford M J, Toth M and Aharonovich I 2016 Quantum emission from hexagonal boron nitride monolayers *Nat. Nanotechnol.* **11** 37
[7] Vaidya S, Gao X, Dikshit S, Aharonovich I and Li T 2023 Quantum sensing and imaging with spin defects in hexagonal boron nitride *Advances in Physics X* **8** 2206049
[8] Gottscholl A *et al* 2020 Initialization and read-out of intrinsic spin defects in a van der Waals crystal at room temperature *Nat. Mater.* **19** 540
[9] Reimers J R, Shen J, Kianinia M, Bradac C, Aharonovich I, Ford M J and Piecuch P 2020 Photoluminescence, photophysics, and photochemistry of theV_B^- defect in hexagonal boron nitride *Phys. Rev. B* **102** 144105
[10] Mathur N, Mukherjee A, Gao X, Luo J, McCullian B A, Li T, Vamivakas A N and Fuchs G D 2022 Excited-state spin-resonance spectroscopy of V_B^- defect centers in hexagonal boron nitride *Nat. Commun.* **13** 3233
[11] Ivády V, Barcza G, Thiering G, Li S, Hamdi H, Chou J-P, Legeza Ö and Gali A 2020 Ab initio theory of the negatively charged boron vacancy qubit in hexagonal boron nitride *npj Comput. Mater.* **6** 41
[12] Benedek Z, Babar R, Ganyecz Á, Szilvási T, Legeza Ö, Barcza G and Ivády V 2023 Symmetric carbon tetramers forming spin qubits in hexagonal boron nitride *npj Comput. Mater.* **9** 187
[13] Babar R *et al* 2024 Low-symmetry vacancy-related spin qubit in hexagonal boron nitride *npj Comput. Mater.* **10** 184
[14] Cholsuk C, Zand A, Cakan A and Vogl T 2024 The hBN defects database: a theoretical compilation of color centersin hexagonal boron nitride *J. Phys. Chem. C* **128** 12716
[15] Shishkin M, Marsman M and Kresse G 2007 Accurate quasiparticle spectra from self-consistent *GW* calculations with vertex corrections *Phys. Rev. Lett.* **99** 246403
[16] Onida G, Reining L and Rubio A 2002 Electronic excitations: density-functional versus many-body Green's-function approaches *Rev. Mod. Phys.* **74** 601
[17] Kresse G and Furthmüller G J 1996 Efficient Iterative schemes for Ab initio total-energy calculations using a plane-wave basis set *Comput. Mater. Sci.* **6** 15
[18] Kresse G and Joubert J 1999 From ultrasoft pseudopotentials to the projector augmented-wave method *Phys. Rev. B* **59** 1758
[19] Perdew J P, Burke S and Ernzerhof M 1996 Generalized gradient approximation made simple *Phys. Rev. Lett.* **77** 3865
[20] Mendelson N *et al* 2021 Identifying carbon as the source of visible single-photon emission from hexagonal boron nitride *Nat. Mater.* **20** 321
[21] Alcántara Ortigoza M and Stolbov S 2022 Thermodynamic stability and optical properties of C-doping-induced defects in hexagonal boron nitride as potential single-photon emitters *Phys. Rev. B* **105** 165306
[22] Li Q, Zhang Q, Bai Y, Zhang H, Hu P, Li Y and Yun F 2021 Deep-UV hexagonal boron nitride (hBN)/BAlN distributed Bragg reflectors fabricated by RF-sputtering *Opt. Mater. Express* **11** 180
[23] Chou S-L, Lin M-Y, Huang T-P, Lin S-Y, Yang M-Z, Lee Y-Y and Wu Y-J 2022 Far-UV spectroscopy of mono- and multilayer hexagonal boron nitrides *Spectrochim. Acta A Mol. Biomol. Spectrosc.* **270** 120849